Applied Nanoscience (2021) 11:1393–1409
https://doi.org/10.1007/s13204-021-01753-3

ORIGINAL ARTICLE

Phytofabrication of cupric oxide nanoparticles using *Simarouba glauca* and *Celastrus paniculatus* extracts and their enhanced apoptotic inducing and anticancer effects

Amulya Giridasappa[1,2] · Dinesh Rangappa[1] · Gopinath Shanubhoganahalli Maheswarappa[3] · Navya Rani Marilingaiah[4] · Chandrashekara Kagepura Thammaiah[5] · Ismail. M. Shareef[2] · Rangappa Kanchugarakoppal Subbegowda[5] · Prasanna Doddakunche Shivaramu[1]

Received: 5 January 2021 / Accepted: 14 February 2021 / Published online: 1 March 2021

Abstract

Cupric oxide nanoparticles (CuO NPs) were phytofabricated utilizing leaf extract of *Simarouba glauca* and aerial extract of *Celastrus paniculatus* and are considered to hold excellent anticancer capability. Synthesized CuO NPs were characterized for their morphology, crystallinity, and structure. The presence of functional groups of phytochemicals on synthesized nanoparticles was validated by Fourier transform infrared spectroscopy (FTIR) analysis. Scanning electron microscopy (SEM) and transmission electron microscopy (TEM) examination reveal the uniform distribution of particles and the average particle size is 35 nm. The anticancer activities on MCF-7 and HT-29 cell lines revealed that CuO NPs synthesized using leaf extract of *S. glauca* (CuO-SG) induced cell death with half-maximal inhibitory concentration (IC_{50}) value of 107.56 µg/mL and 208.57 µg/mL, while CuO NPs synthesized using the aerial extract of *C. paniculatus* (CuO-CP) indicated IC_{50} values of 97.39 µg/mL and 205.11 µg/mL, respectively. To be more precise for anti-cancerous effect, the molecular mechanism was examined in MCF-7 cell line treated with CuO-CP NPs by cell cycle analysis that depicted 75.28% of cell arrest in Sub G_0/G_1 phase and 71.29% of cells were gated in the late apoptotic phase of Annexin V and propidium iodide (PI) compared to control cells. The present work reports in vivo antitumor studies of CuO-CP NPs against Ehrlich ascites carcinoma (EAC) bearing C57 mice for the first time and was examined by variations in growth parameters, biochemical assays, hematological profile, and histopathological analysis. CuO-CP NPs could eliminate oxidants like lactoperoxidase and myeloperoxidase, stimulate reduced glutathione, restore the hematological profile and increase the life span of tumor-bearing mice treated by them in comparison with control.

Keywords Cupric oxide nanoparticles · Anticancer studies · Apoptosis · Cell cycle analysis · Caspase-3 · EAC bearing C57 mice

✉ Ismail. M. Shareef
ismailshareef@acharya.ac.in

✉ Rangappa Kanchugarakoppal Subbegowda
rangappaks@yahoo.com

✉ Prasanna Doddakunche Shivaramu
prasuds@gmail.com

[1] Department of Nanotechnology, Visvesvaraya Technological University, Center for Postgraduate Studies, Muddenahalli, Chikkaballapur 562 010, India

[2] Department of Biotechnology, Acharya Institute of Technology, Bengaluru 560 107, India

[3] Department of Biotechnology, Davangere University, Shivagangotri, Davangere 577 002, India

[4] School of Basic and Applied Sciences, Dayanand Sagar University, Bengaluru 560 111, India

[5] Institution of Excellence, Vijnana Bhavan, University of Mysore, Mysuru 570 006, Karnataka, India

Introduction

Nanoparticles are being emerged as very promising and reliable materials in many applications such as biomedical engineering and cancer therapeutics. Nanoparticles are widely used to develop novel green slurries for use in semiconductors, microelectronics, and optoelectronics industries (Xie et al. 2020; Zhang et al. 2021). They are also employed to develop novel diamond wheels (Zhang et al. 2012) and machining approaches (Zhang et al. 2015) meeting the stringent requirements suggested by high-performance components and devices. With these developed slurries, diamond wheels, and methods (Zhang et al. 2013, 2017) high-performance surfaces are manufactured, which are extremely difficult to be fabricated by conventional technologies (Bai et al. 2017). More importantly, these studies are a landmark for eliminating pollution to the environment induced by traditional manufacturing and industries (Zhang et al. 2020) in which toxic and corrosive slurries are widely adopted (Zhang et al. 2019). Sustainable development of techniques involving biological source for the preparation of nanomaterials for medicinal applications is adopted enormously for the concern of the protection of habitat. The biosynthesis/herbal extracts mediated synthesis of nanoparticles as the spotlight of the intersection of nano-biotechnology, has acquired alarming consideration due to the demanding usage to promote environmentally benign methods in the synthesis of nanomaterials (Baghizadeh et al. 2015). The biological synthesis of nanoparticles is receiving tremendous interest as it is eco-friendly, cost-effective, and consumes less time when compared to conventional methods. Generally, chemical synthesis involves the usage of toxic chemicals and physical synthesis includes the tedious process to be performed. Preparation of nanoparticles by employing natural commodities as a source of reducing and stabilizing factors has been extensively adopted in several fields especially in medicine, mainly due to its low cost, biocompatibility, and non-toxic byproducts (Azizian-Shermeh et al. 2017).

Cancer is the second most principal determinant for death epidemically, according to a recent report of the World Health Organization (WHO 2018), and is described as the proliferation of abnormal cells in a disorganized manner. To treat cancer, various painful methods like surgery, chemotherapy, and radiotherapy have to be undergone. Nevertheless, these regular methods are high priced and have many adverse effects, which limit their utilization. There is an immediate requirement for potent, less expensive, and non-hazardous medication with minimal aftereffects, which are tolerable by the affected (Nagajyothi et al. 2017). Nanoparticles offer exclusive interactions of biomolecules, which are favorable in cancer identification and remedy (Kiessling et al. 2010; Seigneuric et al. 2010).

Copper-based particles are of crucial technological interest and have fascinatingly more considerations for decades because of their excessive conductivity, economical value, and medicinal properties. Copper is one of the six metals of antiquity handled since the prehistoric period. Copper-based nanoparticles have remarkable characteristic features that have made them essential for diverse utilizations in the area of material science, biotechnology, and catalysis (Suárez-Cerda et al. 2017). CuO NPs are widely used in gas sensors, superconductors, magnetoresistance materials, low-cost flat panel displays, spintronics, low-cost solar cells, nano complex materials preparation, antimicrobial, antifungal, antioxidant, anti-inflammatory, anticancer activities, and so on (Baik et al. 2000; Tarasov et al. 2002; Li et al. 2008; Abramov et al. 2009; Cheon et al. 2012; Das et al. 2013; Sivaraj et al. 2014a; Nagaonkar et al. 2015). An exothermic reaction occurs among oxidizing as well as reducing agents in the time of synthesis of CuO NPs (Nethravathi et al. 2015). Technically during the preparation of nanoparticles, metal nitrates are employed by the virtue of their distinctive solubility to comprise a homogeneous blend. Metal nitrates function as oxidizing agents whereas fuel i.e., the phytochemicals of plant content behave as reducing agents for the synthesis of CuO NPs (Ye et al. 1997; Suresh et al. 2015a, b; Naika et al. 2015). Research works are supporting the enhancement in biological activity when CuO NPs were synthesized by biological approach rather than chemical (Rehana et al. 2017; Koca et al. 2018; Verma and Kumar 2019).

In this article, we are reporting the preparation of CuO NPs using the green combustion method with extracts of *S. glauca* and *C. paniculatus.* These two medicinal plants have gained much attention in biological treatment due to their effectiveness, ample availability, and a wide array of secondary metabolites constituted in them. *S. glauca* commonly known as 'Paradise tree' is very much admired for its ethnopharmacological properties. Various genera of this family are used as a remedy for malaria, cancer, worms, viruses, gastritis, ulcer, inflammation, diarrhea, and diabetes, furthermore serves for insecticidal, healing along with tonic activities (Li et al. 2008; Alves et al. 2014). Other than their ethnopharmacological applications, herbs of the *Simaroubaceae* family could be emphasized for chemical assortment as it consists of quassinoids, alkaloids, terpenes, steroids, flavonoids, anthraquinones, coumarins, saponins, mono as well as sesquiterpenes (Tarasov et al. 2002; Barbosa et al. 2011; Alves et al. 2014). *C. paniculatus* is also a conventional medicinal herb with a varied pharmacological specificity. Its effective phytoconstituents comprises triglycerides like palmitooleopalmitin, palmitooleostearin, palmitodiolein, palmitooleolinolein, stearodiolein, triolein as well as dioleolinolein; sesquiterpene alkaloids like celapanin, celapanigin, celapagin; quinone-methide along with

phenolic triterpenoids like celastrol, pristimerin, zeylasterone, and zeylasteral (Kumar et al. 2014, 2015; Azizian-Shermeh et al. 2017). *C. paniculatus* are noted for their benefits over several immunological processes like neurotropic, anti-inflammatory, and antiarthritic (Rajkumar et al. 2007; Harish et al. 2008b; Weng et al. 2013) hypolipidemic (Patil et al. 2010) anti-cancerous (Harish et al. 2008,; Wang et al. 2013) and others.

These two therapeutic plants limit the reactive oxygen species (ROS) present in cancer cells, may function as a favorable inciting material for the formation of NPs and the functional moieties may induce an anticancer effect on these NPs. Because of these facts, the method has been optimized to the synthesis of CuO NPs by maintaining the suitable concentration of copper ions along with leaf and aerial extract. The method applied here is simple, worthwhile, accessible, and sustainable. Hence, a comparative analysis was made to exploit the apoptotic effect of these extracts on breast and colon cancer cell lines in vitro.

Materials and methods

Plant material

Simarouba glauca DC. leaves and *Celastrus paniculatus* Wild aerial parts were collected near the Foundation for Revitalization of Local Health Traditions (FRLHT) campus, Bangalore; Karnataka, India in April 2018 with voucher specimen (120199 & 120198) for herbarium has been deposited in the same Center for Conservation of Medicinal Resources, The University of Trans-Disciplinary Health Science and Technology (TDU). The material surfaces were cleaned using distilled water, shade-dried and then ground by using a blender to obtain a neat powder and preserved in an airtight container at room temperature.

Extraction process

About 20 g of powdered material was concentrated in 200 mL of deionized water in a beaker then kept for boiling for 30 min. Later, the concentrate was brought to room temperature, refined using Whatman filter paper1, and centrifuged to remove undissolved particles. The extracts were stored at 4 °C in screw cap bottles for forthcoming use.

Phyto-synthesis of nanoparticles

Copper nitrate trihydrate (AR) was purchased from Merck and was used to synthesize CuO NPs with a literature method (Nethravathi et al. 2015; Saif et al. 2016) including slight modifications. To 10 mM solution of $Cu(NO_3)_2.3H_2O$, an aqueous extract of the plant (1:2 v/v) was added dropwise and heated up to 80 °C for 5 h with uniform agitation. The mechanism of the reaction was visualized by the variation in the color of fluid from light blue to green and finally appeared brown, thereby clarifying the formation of CuO NPs. The above mixture was brought to room temperature and placed in a pre-heated muffle furnace with a temperature of 400 ± 10 °C for 5 min to make combustion susceptible. This process resulted in obtaining a dark-brown powder which was preserved in sealed containers for forthcoming use.

Characterization

The surface morphology and particle size were studied using Jeol/JEM 2100F TEM operated at 200 kV, 100,000 X magnification, ZrO_2/W (100) field emission gun using LaB_6 as the filament source, fitted with a CCD camera of 0.8 eV emission. Shape and morphological characteristics were examined by employing Hitachi SU1510 variable pressure SEM with an accelerating voltage of 15 kV. The presence of elemental copper and its quantitative composition was determined using Energy Dispersive X-Ray Analysis (EDX). Functional groups and chemical composition were retrieved by noting the spectrum at a wavelength of 400–4000 cm^{-1} from Perkin–Elmer UATR Spectrum Two model FTIR. The optical properties of synthesized CuO NPs were determined employing UV–Vis spectrophotometer (Perkin–Elmer Lambda-750) with 200 to 800 nm wavelength. The phase identification of crystalline material was done by Rigaku Ultima IV, X-ray diffraction (XRD) with Cu-Kα radiation ($k = 0.15406$ nm) at 40 kV and 30 mA.

In vitro studies employing cancer cell lines

Assessment of anticancer activity

Caucasian MCF-7 breast cancer cell line and HT-29 colorectal adenocarcinoma cancerous cells were procured from American Type Culture Collection (Manassas, U.S). The cells were seeded uniformly into plates and sustained in Dulbecco's Modified Eagle's Medium (DMEM) upgraded with 10% fetal bovine serum (FBS), (0.1%) minimal inorganic supplements, penicillin, and streptomycin (10 mL/L) with a humid atmosphere of 5% CO_2 at 37 °C up to confluency.

To estimate the anticancer activity, mitochondrial condition of cancerous cells were evaluated by 3-(4,5-dimethylthiazol-2-yl)-2,5-diphenyltetrazolium bromide (MTT) method, the enzyme called mitochondrial succinate reductase will cleave tetrazolium salts of MTT in viable cells to comprise formazan dye which is disintegrated using Dimethyl Sulfoxide (DMSO) (Mosmann 1983). To commence the process in each well, 100 µL of diluted cell suspension (30,000 cells/well) was incubated at 37 °C for 24 h, and then 100 µL of

different CuO NPs concentrations were treated at 37 °C for 24 h nurtured in 5% CO_2 incubator. Next, 100 µL of MTT (0.5 mg/mL) was supplemented to each well and incubated in dark for 4 h at 37 °C in 5% CO_2 atmosphere. MTT reagent was discarded, DMSO of 100 µL was added and eventually optical density was determined using a microplate reader (SpectraFluor plus, Tecan, US) at a wavelength of 590 nm. The cytotoxicity of cells was indicated as the percent of control to that of the sample.

Substantiation using flow cytometry

For the apoptotic study, cells were cultured in a 6-well plate at 3×10^5 cells/2 mL density for 24 h at 37 °C in 5% CO_2 incubator. Cells were treated with the required concentration of experimental compound then the medium was taken off and transferred to polystyrene tubes. Cells were washed using 1× concentration of Phosphate Buffer Saline (PBS) and recovered using trypsin-ethylene diamine tetraacetic acid. Then cells were harvested by centrifugation at 300×g and washed with PBS. For examination of apoptosis, FITC (fluorescein isothiocyanate) Annexin V Apoptosis Detection Kit (BD Pharmingen) was used. Cells were supplemented with FITC Annexin V (5 µL) with gentle vortex, PI (5 µL), and 1X binding buffer (400 µL) (Thylur et al. 2011). Immediately after addition, BD FAC Calibur Flow cytometer (BD Biosciences, San Jose, CA) supplied with laser (excitation wavelength of 488 nm) and PI as fluorochrome at 585 nm was used for analysis by selecting 10,000 gated events employing Cell Quest Pro Software (Version: 6.0). Only single particles were considered in apoptotic gated events and plotted for Annexin V-PI expression against MCF-7 cells to know the percentage of cells existing in a specific stage. Cell aggregates and doublets formed were not remarked in scattered parameters.

For cell cycle analysis, similar steps of apoptosis studies were followed till centrifugation and then washed with PBS. BD Cycle test Plus DNA Reagent Kit was used to examine this study. Cells were harvested by fixing with 70% ethanol on ice for 30 min, centrifuged and the pellets were dispersed in PBS. Ribonuclease A was added to ensure deoxyribonucleic acid (DNA) gets stained followed by 400 µL of PI. After incubation for 10 min, the results were analyzed utilizing Fluorescence-activated cell sorting (FACSCalibur, BD Biosciences, USA). PI histogram of 10,000 gated cell singlets differentiates cells at Sub G_0/G_1, G_0/G_1, S, and G_2/M phases each in control and synthesized CuO NPs.

Caspase-3 expression study was performed as a marker analysis for spotting protease that gets stimulated in the course of an early stage of apoptosis in cancerous cells. Caspase-3 are required for DNA fragmentation, similar steps of cell cycle analysis were accomplished up till cell fixing, and then it was pursued by the inclusion of 500 µL of cytofix for 10 min. Later, rinsed using 0.5% bovine serum albumin and mixed thoroughly in 20 µL of Caspase-3 antibody. The sample was incubated in the dark at room temperature for 30 min. An eventual wash using 0.5 mL of 1X PBS with 0.1% sodium azide was conducted to scrutinize by flow cytometry.

Evaluation of in vivo anticancer efficacy of CuO-CP NPs

Animal use and care

A healthy horde of C57 mice aged 5–7 weeks and body weight ranging between 28 and 32 g were employed in the study. They were allowed to acclimatize to laboratory conditions with the temperature maintained at 22 ± 3 °C and were placed in polypropylene cages with sawdust bedding, maintained at animal house facility at Acharya & BM Reddy College of Pharmacy, Bengaluru, Karnataka, India. The mice were provided with standard food, water *ab libitum*, 12-h light–dark time phase, and were let to habituate for a week before the commencement of the experiment. The leftover food and water were changed every morning, sawdust once in three days, to ensure hygiene. The investigation was authorized by Institutional Animal Ethics Committee with registration No.: 997/c/06/CPCSEA.

Single oral dose and induction of tumor

The acute oral toxicity was performed following OCED test guideline 425 on C57 mice. Animals were unfed for 12 h and then orally administrated with CuO-CP NPs at graded doses from 500, 1000, and 2000 mg/kg body weight using oral gavage. The gross appearances of animals were observed immediately for 30 min, intermittently for 1, 4, and 24 h. Consequently, the animals were observed once a day for 21 days for any behavioral, anorexia, circadian rhythm, and depression of the central nervous system. There was no mortality or abnormal lesions observed at 2000 mg/kg dose and hence it was considered as median lethal dose (LD_{50}). One-twentieth and one-fortieth of peak safe dose of CuO-CP NPs, verified by acute toxicity were chosen for the in vivo analysis. The parent inoculum of EAC cells was received by the courtesy of Amala Cancer Research Centre, Trissur, India. To induce ascites tumor in mice, 2×10^6 cells per mouse were propagated through intraperitoneal injection (fortnightly). Donor mice harboring 7–8 days old ascitic tumor were extracted for EAC cells and the collected cells were counted by haemocytometer using normal saline (0.9%) dilution to adjust the cell count to 1×10^6 cells/mL. Later, 0.2 mL volume of cells was implanted to each recipient mouse excluding normal control which received just normal saline.

In vivo estimation of EAC cell growth inhibition

For the subacute studies, six groups consisting of eight animals each were assigned randomly. The day when EAC was implanted in these animals were considered as Day 0. Eventually, CuO-CP NPs and standard treatment were established from Day 1 and the process remained till 21 days. Group-I animals were considered as negative control and were orally mainlined with normal saline. Group II-VI signifies the mice harboring EAC, Group II which served as positive control and were the untreated mice. Group III and IV indicated low (50 mg/kg BW) and high (100 mg/kg BW) doses of CuO-CP NPs. Group V was administered with Hesperetin (30 mg/kg BW), dietary flavanones, and Group VI with 5-Fluorouracil (20 mg/kg BW), and these medications used in chemotherapy were both taken as standard. When the last dose was administered, four animals from the individual group were unfed for 18 h, and blood was withdrawn from all of them by retro-orbital plexus and examined for the hematological profile. The same animals were sacrificed and tissues such as kidney, liver, and spleen were gathered for biochemical and histopathological examination. The surviving animals of the individual group were continued with the provision of sufficient food and water to know their life expectancy and related parameters.

Evaluation of hematological and biochemical parameters

With an interest to know the potency of CuO-CP NPs on animal research in vivo, the measurement of changes in body weight, mean survival time (MST), and percentage increase in life span (%ILS) were performed. A hematology analyzer (Nihon Kohden Celltac α MEK 6500 K, Europe) was used to assess the hematological profiles such as red blood cell (RBC), white blood cells (WBC), and hemoglobin (Hb) content from the blood drawn of each group. The biochemical capability of CuO-CP NPs and standard on both normal and EAC bearing mice was carried out using 10% w/v tissue homogenate of the liver which was soaked in ice-cold physiological saline and then in 10% KCl, persuaded by centrifugation at 1500 rpm for 12 min and 4 ºC. The retrieved supernatant was assessed for cellular contents of malondialdehyde (MDA), myeloperoxidase (MPO), and reduced glutathione (GSH). Ellman's reagent was mainly used to estimate GSH (Ellman 1959), MDA, a subsidiary compound of lipid peroxidation was evaluated as per Ohkawa et al. 1979 and MPO by Mullane et al. 1985.

Histopathological diagnosis

Tissue samples of kidney, liver, and spleen of normal and CuO-CP NPs treated mice were kept firm with 10% v/v neutral buffered formalin. Subsequently, hydration and dehydration cycles were conducted with xylene and ethanol, the specimens were embedded with paraffin. Then ultra-fine sections of 5 µ thickness were made and stained using haematoxylin and eosin to observe under a microscope which aids the histopathological examination.

Statistical analysis

Analysis of variance (ANOVA) of observed data was performed using Ducan's multiple range test (DMRT) by using the Statistical Package of Social Science (SPSS) of windows version 11.5, IBM Corporation, USA. The triplicate samples values of the anticancer activity are presented as mean ± standard deviation, $P \leq 0.05$ was taken into account as statistical significance.

Results and discussions

UV–Vis spectrophotometric analysis

In the reaction mixture, the disappearance of pale blue color and the occurrence of brown are the symbolic evidence of the composition of phytofabricated CuO NPs (See data in supplementary Fig. S1). This on heat treatment converted CuO NPs, which showed the absorbance peaks at 276 nm and 278 nm in the UV–Vis spectrum and are in good agreement with similar research reported (Sivaraj et al. 2014a; Meghana et al. 2015; Gopinath et al. 2016; Berra et al. 2018). Additionally, copper exhibits spectrum because of surface-enhanced optical aspects between sp-conduction band and d-transition band (Suresh et al. 2016).

FTIR analysis

Several phytochemicals with varying functional groups are present in the plant extracts, behaved as stabilizers, and/or capping agents. These functional groups are identified by utilizing FTIR spectroscopy (Fig. 1). The correlating transmittance peaks appearing in 3219, 2923, 2111, 1599, 1321, 1207, 1020, 729, and 456 cm^{-1} for CuO-SG and 3396, 1787, 1635, 1348, 874, 834, and 474 cm^{-1} for CuO-CP were identified using FTIR. Broad transmittance obtained at 3219 and 3396 cm^{-1} was accredited to hydroxyl (–OH) groups (Rao 1963), resembling the existence of phenolics or amino acids. A noticeable peak at 2923 cm^{-1} and a minor peak at 2111 cm^{-1} is attributable to asymmetrical C–H stretch vibrations of alkane and alkyne (Arya et al. 2018). Transmittance at around 1787 and 1635 cm^{-1} was attributed to the oscillation of carbonyl (C=O) relating to a stretch of amide group and peak at 1599 cm^{-1} is due to C=C stretch of the aromatic ring (Ahmed et al. 2005). Peaks at 1348, 1321, 1207, 1020,

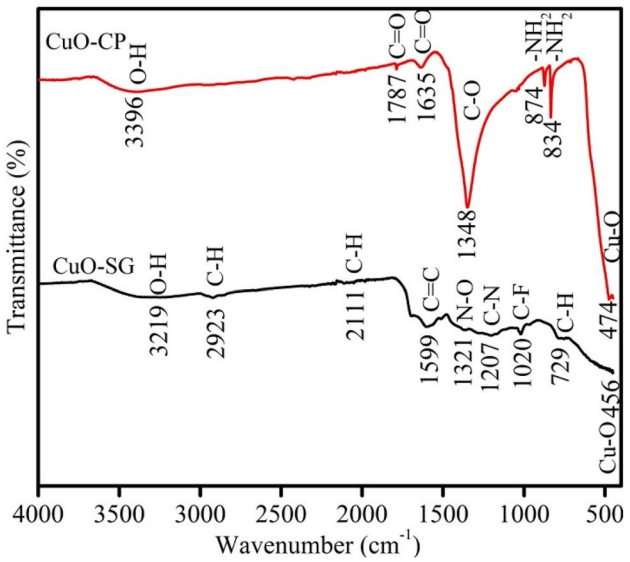

Fig. 1 FT-IR spectra of phytofabricated CuO-SG and CuO-CP NPs

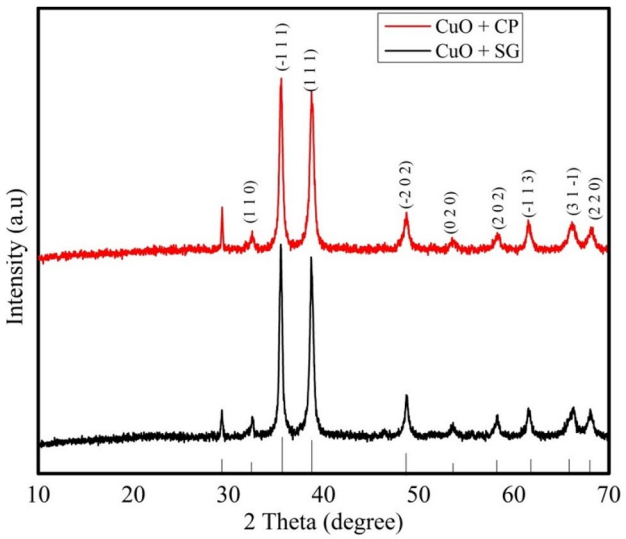

Fig. 2 XRD patterns of as prepared CuO NPs using extracts of *S.glauca* and *C.paniculatus*

874, 834, and 729 cm^{-1} could be due to the existence of various functional groups of phytochemicals such as C–O stretch of polysaccharides or alcohol, N–O stretch of nitro, C–N stretch, C-halo (Li et al. 2004; Ramamurthy and Kannan 2007; Hassanien et al. 2018). Peaks with Cu–O stretch at 474 and 456 cm^{-1} were also observed in the spectra (Sivaraj et al.). In addition, the absence of a peak around 610 cm^{-1} indicates that Cu_2O is not formed in the process, confirming that the sample consists of CuO NPs (Vishveshvar et al. 2018).

XRD studies

XRD patterns of CuO NPs revealed main diffraction peaks with 2θ = 32.50°, 35.50°, 38.68°, and 48.81° for CuO-SG and 2θ = 32.54°, 35.54°, 38.73°, and 48.66° for CuO-CP which correspond to the (0 1 1), (1 1 −1), (1 1 1), and (2 0 −2) miller indices, respectively (Fig. 2). The sharp intensity and narrow width peak confirm the crystal structure formation and were in good accord with Joint Committee on Powder Diffraction Standards card (No. 48-1548) (Ethiraj and Kang 2012; Hwa et al. 2019). The pattern represents the pure monoclinic structure of CuO NPs with space group 15**:** C12/c1, unique-b,cell-1. The average crystalline size was resolved using Debye–Scherrer formula $D = K\lambda/\beta\cos\theta$ and was valuated to be about 35 nm. The absence of additional peaks in XRD pattern indicates purity of CuO NPs. Based on the results obtained the extracts CuO-SG and CuO-CP induced the restraint on the crystalline size of the sample.

Evaluation of morphology

The surface morphology and structure of CuO-SG and CuO-CP NPs were acquired using SEM and findings are presented in Fig. 3. We could observe that spherical shape CuO NPs as indicated in Fig. 3A and B. The outline of Energy Dispersive X-ray Spectroscopy indicated the existence of only C, Cu, and O elements. The signal of copper relatively at 1, 8 & 9 keV and oxygen signal at 0.5 keV followed by carbon were observed. This demonstrates a qualitative and quantitative chemical composition of CuO NPs. The above findings were in good accord with those of (Nasrollahzadeh et al. 2015).

TEM results revealed the polydispersed and spherical shape of phytofabricated CuO NPs and their morphology as shown in Fig. 4. The size, shape, and crystallinity were known from the insight of images and were found to be 30–40 nm in diameter which was in agreement with XRD analysis. It is also observed that obtained CuO NPs have agglomerated appearance and were prominently embedded in filaments, the evidence was similar to previous research conducted (Sivaraj et al. 2014b; Nethravathi et al. 2015). Thus, natural compounds, which exist in leaf and aerial extracts could stabilize, in addition to the formation of CuO NPs. The outcome of this analysis was favorable with SEM evaluation.

In vitro anticancer activity

This contemporary research work deals with cytotoxic studies of phytofabricated CuO-SG and CuO-CP NPs and is exhibited as the percentage of inhibition of MCF-7 and HT-29 cell lines in a concentration-dependent manner. The

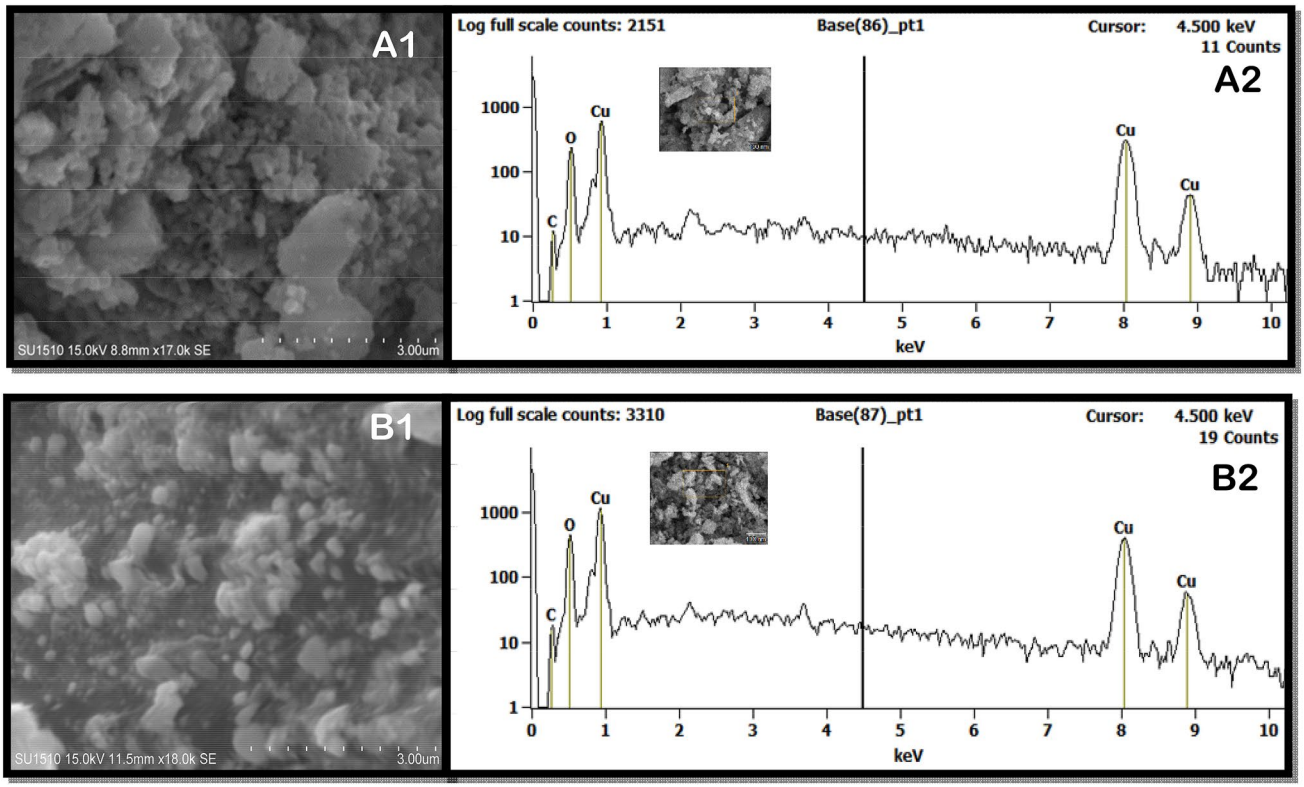

Fig. 3 SEM monographs of synthesized CuO-SG (A1) and CuO-CP (B1) NPs; EDS spectrum captured from synthesized CuO-SG (A2) and CuO-CP (B2) NPs

cells treated with phytofabricated CuO NPs showed shrinkage, retraction, membrane blebbing, protein injury, and cytoplasmic vacuolation which were distinguished evidently due to MTT stain taken up by mitochondria in viable cells. The several concentrations of CuO NPs varying from 10 µg/mL to 320 µg/mL inhibited the cell growth following the 24 h of treatment. The half-maximal inhibitory concentration (IC_{50}) was estimated to be 107.56 ± 1.87 and 97.39 ± 0.48 µg/mL conjointly with 208.57 ± 0.66 and 205.11 ± 0.39 µg/mL against MCF-7 and HT-29 cell lines for CuO-SG and CuO-CP NPs, respectively as shown in Fig. 5. This indicates a less confluent stage of cells after their dosage and their capability to destroy cancer cells.

It is certain from Table S1, that the inhibition on the growth of these cancerous cells was dependent on the concentration of CuO-SG and CuO-CP NPs. The synthesized CuO NPs showed the better arrest of cell growth in MCF-7 cells correlated to HT-29 cell lines, as they could easily penetrate cancer cells by their unique properties and thereby demonstrating their potential application as an anticancer agent. The intensified activity as a potent anticancer drug by synthesized CuO NPs can also be attributed due to the presence of secondary metabolites in these extracts. Our results propose that they are reliable with differential cytotoxic efficiency of the synthesized CuO NPs which were in good accord with similar reports (Sivaraj et al. 2014b; Ramaswamy et al. 2016; Sulaiman et al. 2018) analyzed using a different panel of cancer cell lines and the biological sources.

Among the four treatments, CuO-CP NPs that were used to control the growth of MCF-7 cell lines was considered for further examinations to interpret their effect on the morphology of cells during apoptosis, as it possessed a slight high phenomenal IC_{50} value compared to the rest and there are no reports on apoptosis and cell cycle evaluation using this bio component.

FITC annexin V-PI-based FACS analysis

The bunch of cells subjected to apoptosis can be quantitatively determined from FITC-Annexin V analysis marked by disrupted membrane symmetry of cells. In cell membranes, a phospholipid called phosphatidylserine (PS) is exposed externally in apoptotic cells which are attracted by Annexin V. PS helps to retain shape and selective permeability of the cell gets translocated during apoptosis. A probe called PI will differentiate non-viable and viable cells. The CuO-CP NPs possessing a half-maximal inhibitory concentration of 97.39 ± 0.48 µg/mL on the MCF-7 cell line was used to check the Annexin V-PI expression as presented in Fig. 6 and their values of percent of cells gated after 24 h

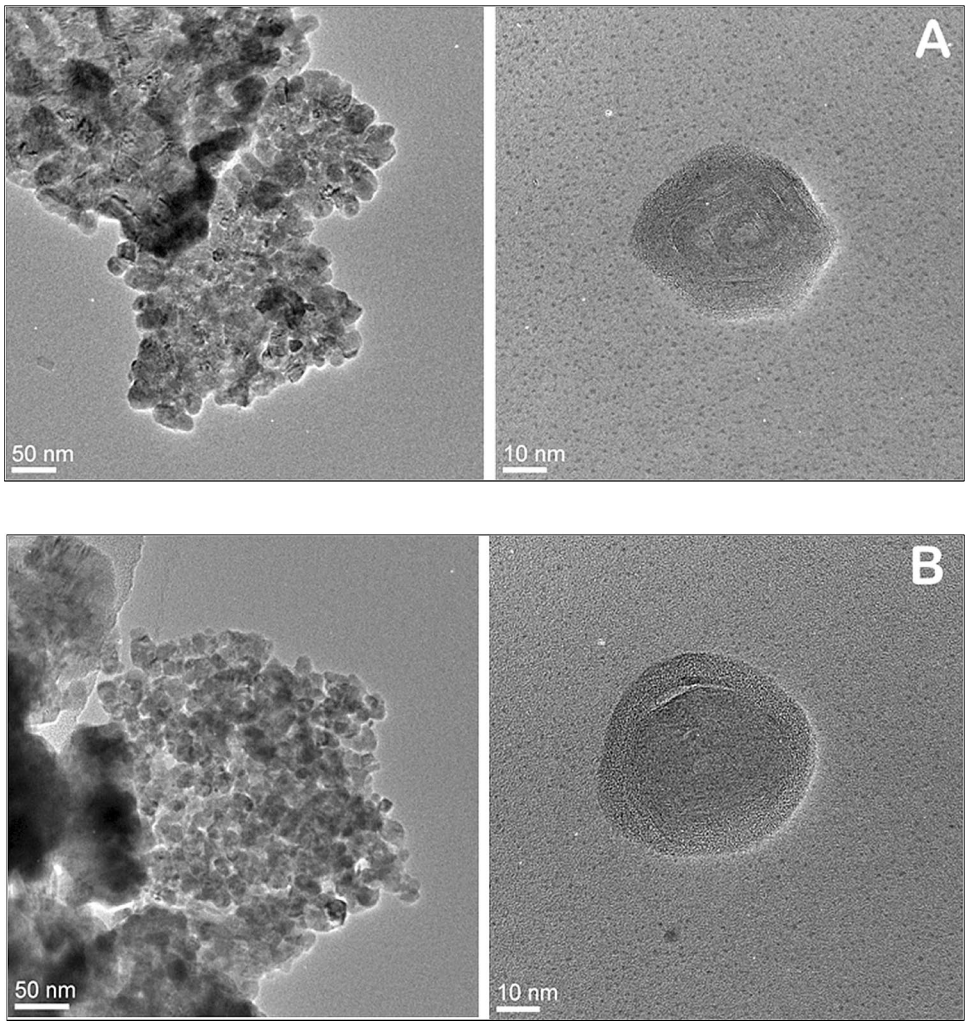

Fig. 4 Captured TEM images of synthesized CuO-SG (A) and CuO-CP (B) NPs

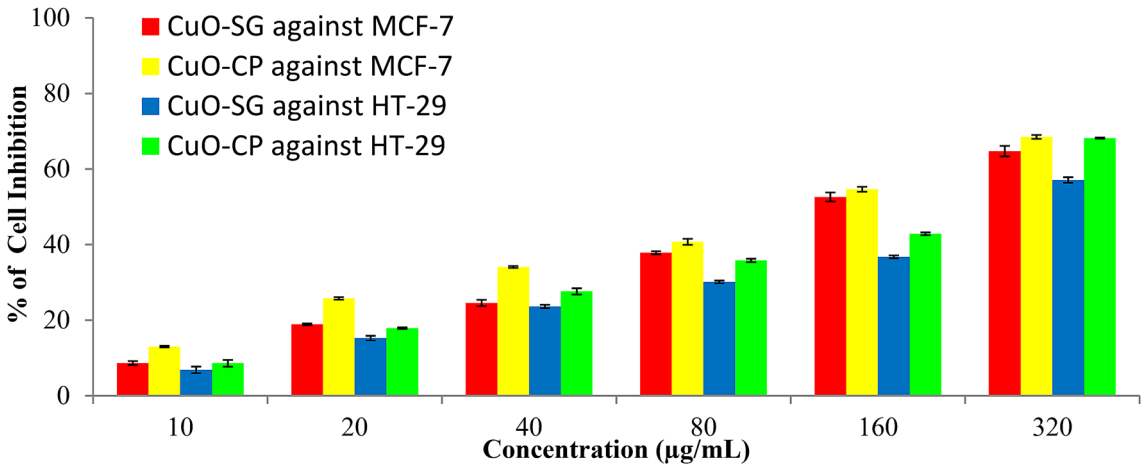

Fig. 5 Percentage inhibition of MCF-7 and HT-29 cell lines by CuO-SG and CuO-CP NPs

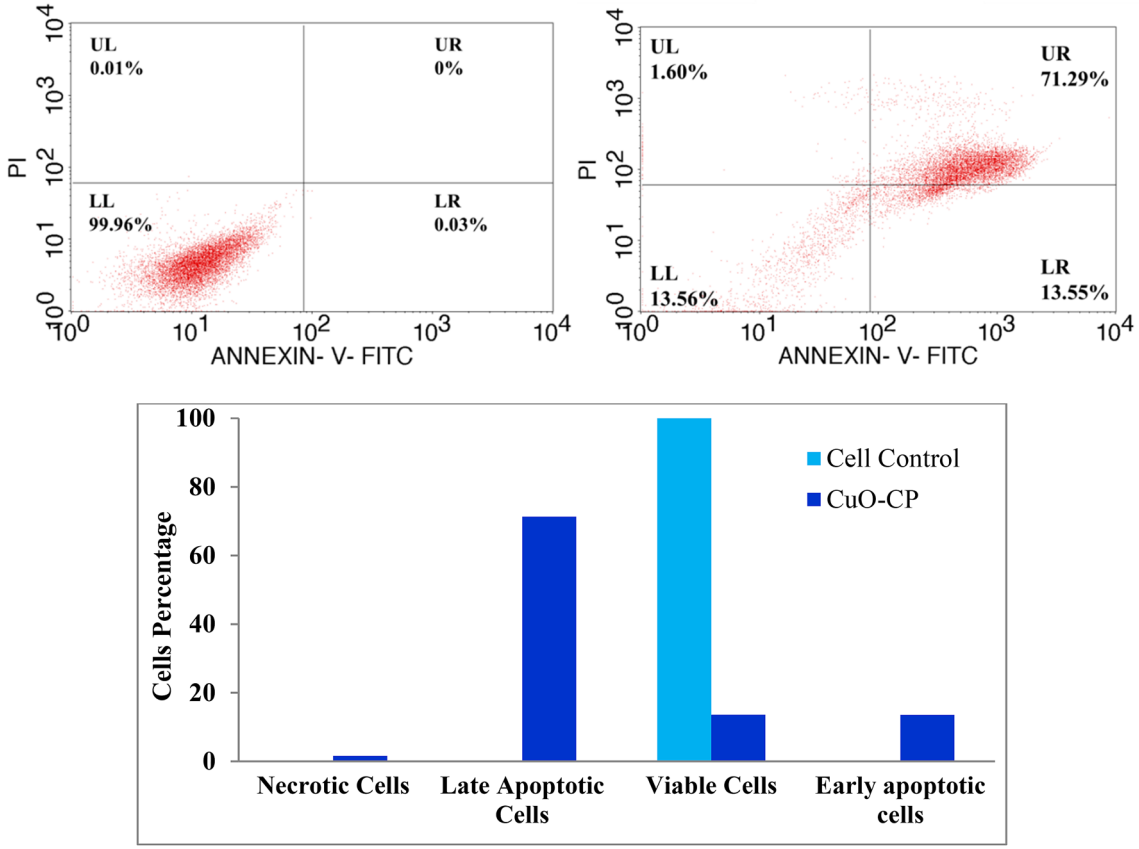

Fig. 6 Quadrants showing Annexin V-PI expression study in terms of percentage of gated cells in cell control and CuO-CP NPs on MCF-7 cell line and overlay of results in form of bar graph

incubation are illustrated along with control. It is indisputable from Fig. 6 that 99.96% of active cells were noticed in control indicating viable cells (Lower Left region) whereas cells treated with CuO-CP NPs has 71.29% of cells in late apoptotic stage (Upper Right region), 13.56% in viable, 13.55% in early apoptotic (Lower Right region) and 1.60% of cells in necrotic stage (Upper Left region) signifying that CuO-CP NPs could proficiently induce apoptosis. The p53 tumor suppressor gene determines the fate of cells, if there is DNA damage, p53 will activate the senescence system to avoid the increase of precancerous cells, phosphorylation of p53-serine 46 kinase triggers proapoptotic genes causing cell death by suicide mechanism (Sari et al. 2018). Our results were similar to these reasons mentioned along with the study conducted by (Kumar et al. 2018; Ray et al. 2019) as CuO-CP NPs effect on MCF-7 cell lines, worked both by the intrinsic and extrinsic pathway of apoptosis and hence accomplished Caspase-3 activity.

Cell cycle analysis using propidium iodide

The cell cycle evaluation was performed to investigate whether the apoptotic cell death was due to the inhibitory effect of synthesized CuO NPs on DNA content in various cell cycle phases. Despite DNA damage, there will be a discontinuous DNA replication to mitosis as a consequence of failure to control the checkpoint stage that occurs in the case of cancer cells which helps them to grow further. This analysis can be used to demonstrate the significance of phytofabricated CuO-CP NPs on the MCF-7 cancer cell cycle to the checkpoint stage, which helps to inhibit the cells from entering the next phase in case of DNA damage.

The MCF-7 cell lines were administered with phytofabricated CuO-CP NPs possessing a half-maximal inhibitory concentration of 97.39 ± 0.48 µg/mL for 24 h, stained with PI and subsequently analyzed as shown in Fig. 7**.** The dot plot was performed using side scatter (SSC) against forward scatter (FSC) with the same set of singlet cells gated for both control and CuO-CP NPs. The shape and granularity of cancer cells were significantly good for control as they are viable whereas in case of CuO-CP treatment, the shape, and granularity were damaged due to anticancer potential possessed by them on MCF-7 cells. This can be observed in the dot plot where a bunch of dead cells is moving downwards in Fig. 7B.

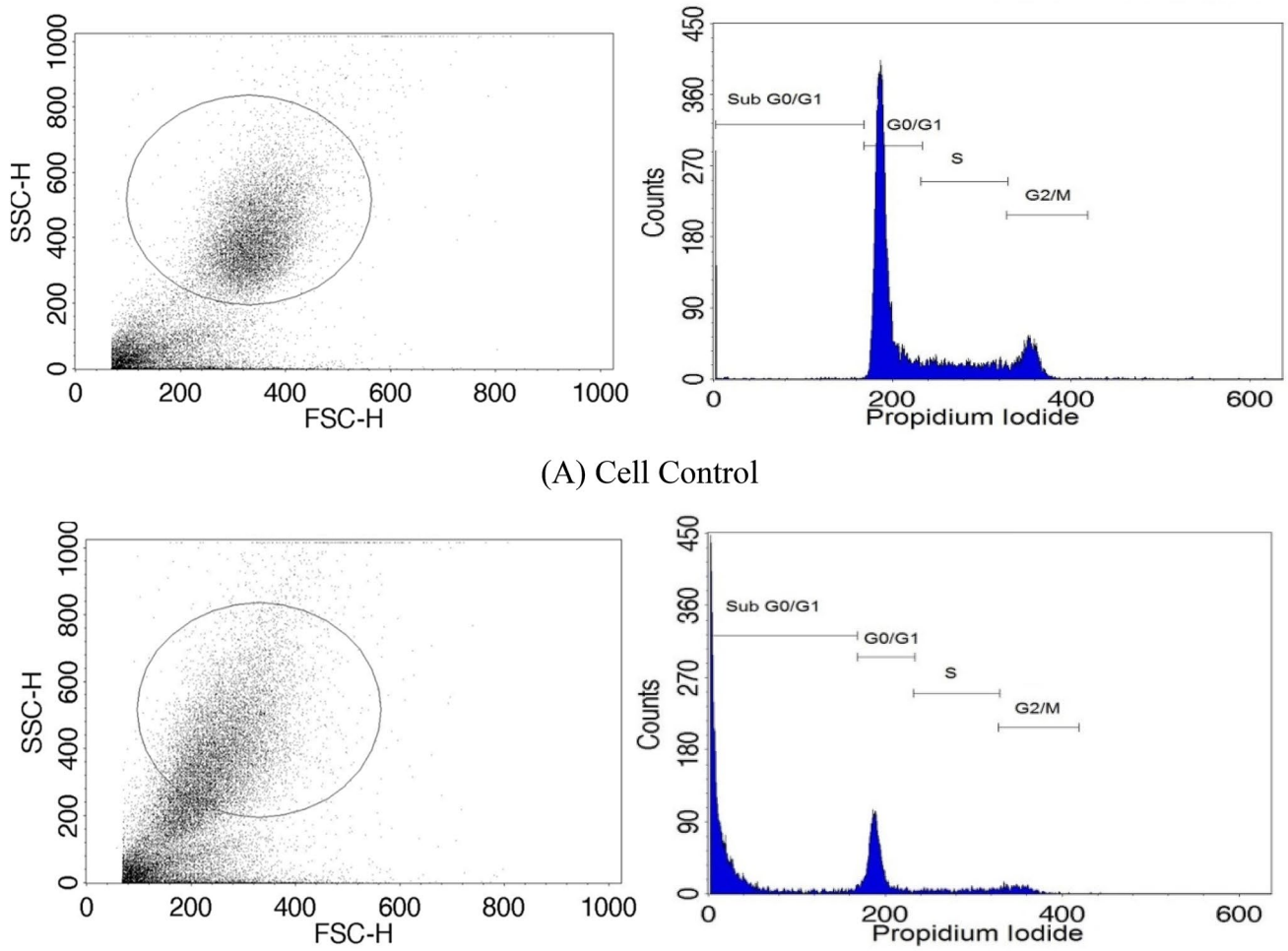

Fig. 7 Percentage of cells arrested in Cell Cycle Analysis of phytofabricated CuO NPs (**B**) and control cells (**A**) against MCF-7 cells employing BD FACS Calibur. Dot plot and PI histogram of 10,000 gated Cell singlets for each sample differentiates cells at the Sub G_0/G_1, G_0/G_1, S, and G_2/M phases. Gating of cell cycle stages is almost accurate and were accomplished by operating system (Cell Quest Software, Version 6.0)

By considering the results from the statistical data of cell cycle (Fig. S2), we can interpret that in G_0/G_1 phase had 65.75% and 17.48% of cells, in S phase 18.32% and 4.10%; 12.86% and 3.38% in G_2/M phase and Sub G_0/G_1 phase also known the apoptotic/cell debris phase has 3.48% and 75.28% of cells arrested in untreated cell control and phytofabricated CuO-CP NPs, respectively. It indicates that maximum cells were present in G_0/G_1 phase for cell control, indicating the viability of cancer cells while phytofabricated CuO NPs had a majority of cells in Sub G_0/G_1 phase signifying elevation in DNA fragmentation in them. CuO-CP-treated cells also show the decreased amount of cells in the S and G_2/M phase, which indicates that the cells could pass through G_0/G_1, S, and G_2/M phase but had got upregulated in apoptotic phase (Sub G_0/G_1). This process of cell arrest in the Sub G_0/G_1 phase of our study was similar to research performed by (Namvar et al. 2014; Mathuram et al. 2016). There are also reports related to cell arrest in the G_1, S, and G_2/M phase of the cell cycle (Ray et al. 2019; Rajashekaraiah et al. 2020). The molecular mechanism behind this upregulation in the Sub G_0/G_1 phase of CuO-CP NPs was confirmed by performing apoptotic protein Caspase-3 assay using flow cytometry.

Expression of caspase-3 in breast cancer cells

In this investigation, the synthesized CuO-CP NPs were utilized to monitor Caspase-3 expression on the MCF-7 cell line. Caspase-3, the terminal factor of apoptosis, is triggered by upstream caspase-8 and caspase-9, and because it functions as a junction point for several

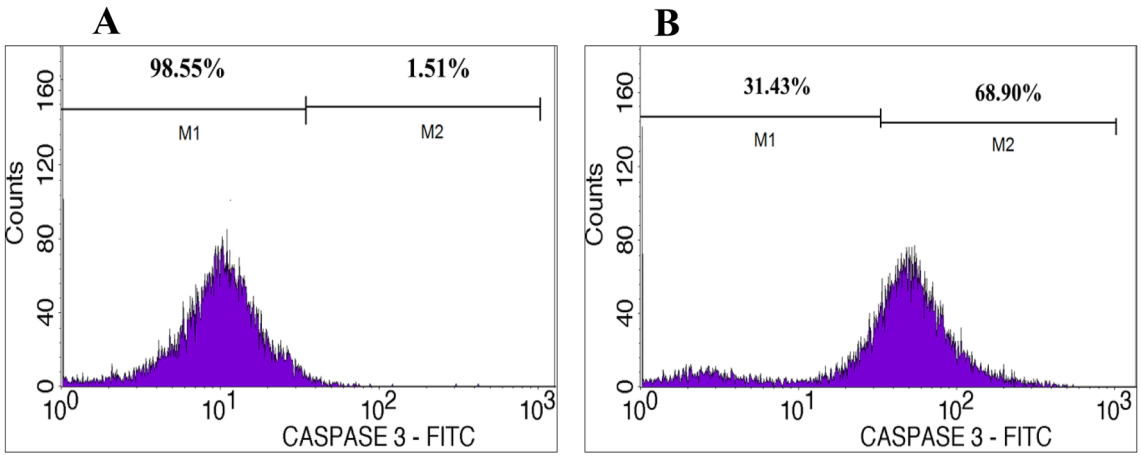

Fig. 8 CASPASE-3 expression study of Cell control (**A**) and phytofabricated CuO NPs (**B**) against the MCF-7 cells employing BD FACS calibur, Cell Quest Pro Software (Version: 6.0)

signaling pathways, it is extensively employed as a control device in apoptosis assay (Kumar et al.).

The histogram of Caspase-3-FITC as indicated in Fig. 8 of the gated MCF-7 singlets, differentiates cells at M1 and M2 phases wherein M1 interpolates negative expression were seen as viable cells and M2 indicates the positive expression were observed in apoptotic cells. These results obtained were similar to the findings of (Dugo et al. 2017; Kumar et al. 2018; Sari et al. 2018; Ray et al. 2019; Thenmozhi 2020). The observation in statistical data by flow cytometry suggests that in MCF-7 cells administered with phytofabricated CuO-CP NPs, the appearance of Caspase-3 was less in untreated cell control with 11.22 Mean Fluorescence Unit (MFU) as to the synthesized CuO NPs with IC_{50} concentration 97.39 ± 0.48 µg/mL had 53.81 MFU. The result proposes a possible connection between apoptosis induced by synthesized CuO-CP NPs and the activation of Caspase-3 proenzyme connected with the initiation of death cascade by both intrinsic and extrinsic pathways. The increase in Caspase-3 protein is correlated to an increase in cells in the late apoptotic stage mediated with CuO-CP NPs on MCF-7 cell lines and thereby inhibits their proliferation.

In vivo growth and survival threshold of C57 mice

By the phenomenal in vitro anticancer potency of synthesized CuO Nps from *S. glauca* and *C .paniculatus*, it was imperative to further investigate its ability to destroy cancer cells in in-vivo models. During acute oral toxicity study, no clinical indications of toxicity were discovered in any of the animals used in the experiment up to the dose of 2 g/kg BW and hence 50 mg/kg BW and 100 mg/kg BW of CuO-CP NPs were used to test the anticancer activity along with standard Hesperetin and 5-Fluorouracil (5-FU). As in when days passed, there were noticeable differences in the external appearance of animals in specified groups. From a week onwards, due to the buildup of ascitic fluid in EAC bearing mice, the body weight increased more vigorously when compared to normal C57 mice.

The body weight, MST, and %ILS of animals in each group are shown in Table 1. A significant ($p < 0.001$) decrement was observed in the bodyweight of CuO-CP NPs treated EAC mice compared to EAC control. The animals dosed with 100 mg/kg BW CuO-CP NPs and 5-FU had weights nearer to normal mice. Also, supplying EAC bearing mice with a daily intake of CuO-CP NPs (100 mg/kg) increased their MST significantly ($p < 0.001$) to

Table 1 Morphological effect of CuO-CP NPs on body weight and survival threshold in laboratory mice

Groups	Normal control	EAC control	EAC + CuO-CP NPs (50 mg/kg BW)	EAC + CuO-CP NPs (100 mg/kg BW)	EAC + Hesperetin (30 mg/kg BW)	EAC + 5-FU (20 mg/kg BW)
Gain in body weight (g)	11.12 ± 0.27**	20.6 ± 1.38***	16.3 ± 1.41***	12.83 ± 0.58***	14.66 ± 0.75***	12.33 ± 0.85***
MST (days)	26.97 ± 2.05**	13.38 ± 0.94***	20.63 ± 1.17***	23.88 ± 1.23***	21.13 ± 1.18***	26.88 ± 0.63***
% ILS	–	–	54.18	78.47	57.92	100

Values are expressed in mean ± S.E.M. ($n = 8$), ** $p < 0.01$ and *** $p < 0.001$ compared to negative control group. Statistical analysis was done by one-way ANOVA followed by Dunnett's post test

23.88 ± 1.23 days, along with %ILS of 78.47% when correlated to EAC control. This indicates that CuO-CP NPs were effective in controlling the growth morphology of mice injected with EAC and could trace the animal back to their normal life. These findings were found similar as nanoparticles could indicate the direct cytotoxic effect of MycoAuNPs on cancer cells as illustrated from in vivo studies (Munawer et al. 2020).

Impact on hematological parameters

The hematological parameters of EAC harboring mice were observed to be significantly ($p < 0.001$) different compared to normal mice and can be summarized in Table 2. Due to disorder in the immune system, WBC was found to be high and anemic conditions could have depleted the levels of RBC and Hb in the EAC control group. Oral dosage of CuO-CP NPs has aided the EAC bearing mice to reduce the WBC content to $6.00 \pm 0.30 \times 10^3$/µL and restore RBC and Hb levels to $5.41 \pm 0.19 \times 10^6$/µL and 12.04 ± 0.56 g/dL which was almost equivalent to the results of 5-FU administered mice. Anticancer medicines alter the physiological properties to cause proper transportation through restricted constrictions, allows the interchange of Hb to improve oxygen uptake, and favors persistent RBC survival in systematic circulation (Wadhwa et al. 2019). There is evidence that after dosing an anticancer agent exhibited a protective effect on the hematopoietic system by the turnaround of total WBC, RBC cells, and Hb content in EAC harboring mice toward the measure of normal group animals (Uddandrao et al. 2019) which supports the current investigation. Thus, treatment of CuO-CP NPs in laboratory animals induced with cancer can help to recapitulate the hematological parameters to the conditions as seen in normal mice.

Biochemical analysis for oxidative stress measurement

The prominence of antioxidant enzymes in normal and EAC induced mice were estimated by measuring the concentration of GSH, MDA, and MPO in tissue homogenate of animals in each group. The biochemical activities indicating the oxidative stress caused due to injecting EAC, treatment with CuO-CP NPs as well as standard in experimental animals are depicted in Fig. 9. It indicates the considerable reduction in levels of GSH in EAC bearing mice to 1.440 ± 0.06 mg/mL but increased as the administration of CuO-CP NPs raised. Under abiotic and biotic stress conditions, excess generation

Table 2 Anticancer capability of CuO-CP NPs on hematological parameters in laboratory mice

Groups	Normal control	EAC Control	EAC + CuO-CP NPs (50 mg/kg BW)	EAC + CuO-CP NPs (100 mg/kg BW)	EAC + Hesperetin (30 mg/kg BW)	EAC + 5-FU (20 mg/kg BW)
RBC (10^6/µL)	6.06 ± 0.05***	2.81 ± 0.21**	4.06 ± 0.18 ***	5.41 ± 0.19 ***	4.45 ± 0.26 ***	5.90 ± 0.01***
WBC (10^3/µL)	4.73 ± 0.12***	13.33 ± 0.29**	8.73 ± 0.27 ***	6.00 ± 0.30 ***	7.70 ± 0.50 ***	5.74 ± 0.09***
Hb (g/dL)	12.68 ± 0.05***	6.823 ± 0.38**	9.570 ± 0.28 ***	12.04 ± 0.56 ***	11.26 ± 0.48 ***	12.52 ± 0.04***

Values are expressed in mean ± S.E.M. ($n = 8$), ** $p < 0.01$ and *** $p < 0.001$ in contrast to negative control group. Statistical analysis was performed by one-way ANOVA followed by Dunnett's post test

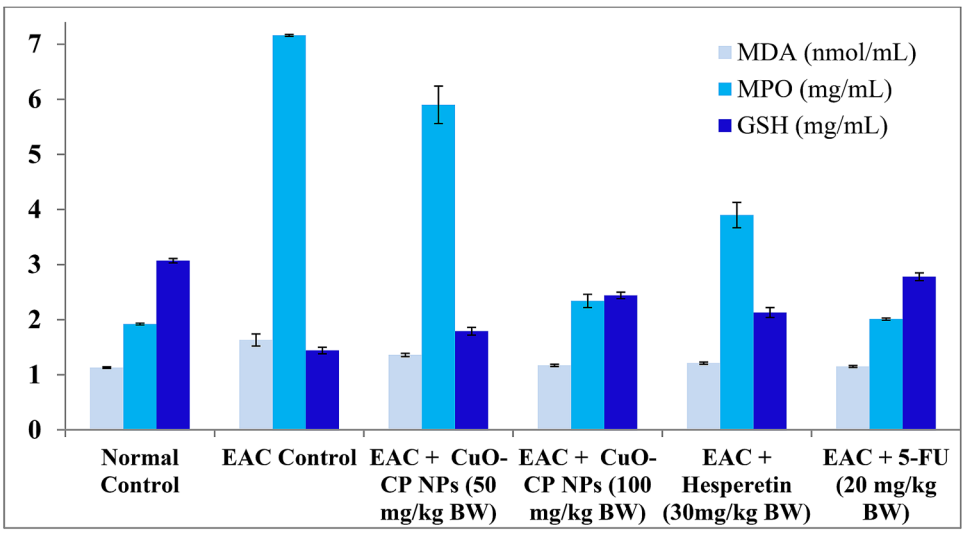

Fig. 9 Biochemical activities of CuO-CP NPs on MDA, MPO and GSH in tissue homogenate of specified animal groups. Values are expressed in mean ± S.E.M. ($n = 8$), * = $p < 0.05$, ** = $p < 0.01$ and *** = $p < 0.001$ compared to negative control group. Statistical analysis was done by one-way ANOVA followed by Dunnett's post test. MDA: Malondialdehyde, MPO: Myeloperoxidase, GSH: Reduced glutathione

of ROS is encountered which can damage the cell and its organelles. To prevail over these harmful oxidants, one of the most efficacious antioxidants GSH, present in animal tissue is utilized. GSH is a fundamental endogenous non-enzymatic antioxidant, which neutralizes free radicals associated damage (Uddandrao et al. 2019). The GSH values obtained in the present study were parallel with Karmakar et al. 2013, it describes the value of reduced GSH being lowered in cancer-bearing mice, which might be because of its usage, by the enormous amount of free radicals.

The levels of endogenous MDA and MPO were significantly ($p < 0.01$) increased in the EAC control group to 1.635 ± 0.11 nmol/mL and 7.167 ± 0.17 mg/mL correlated with the normal control group, nevertheless they were reduced in the group treated with CuO-CP NPs exhibiting values of 1.178 ± 0.02 nmol/mL and 2.347 ± 0.12 mg/mL. MDA is a reactive aldehyde and is one among different responsive electrophile species that bring about cellular toxicity (Elsayed et al. 2020). The disturbance originated in membrane or storage lipids due to the redundancy of ROS induces peroxidation and leads to disruption in biomembranes. Lipid peroxidation invokes the production of ROS and subsequently promotes the level of MDA which activates cancer in liver and kidney tissues (Karmakar et al. 2013). MPO an oxidoreductase reacts with hydrogen peroxide and chloride ions to release hypochlorous acid which can activate irrevocable nonspecific modifications in major biomolecules. The outcome of biochemical analysis performed was consistent with the work done by (El-Far et al. 2019) demonstrated an increase in the antioxidant like GSH status following CURnp1 and CURnp2 treatment of EAC tumor as well as decreased cellular levels of MDA.

Effect of CuO-CP NPs on histology of various organs

Toxic potential of CuO-CP NPs on organs like kidney, liver, and spleen was determined by gross and histopathological examination and also for normal, EAC bearing mice along with standard groups under study, are as illustrated in Fig. 10. Light microscopic analysis revealed that the group of CuO-CP NPs and 5-FU treated mice exhibited well-adjusted histological architecture as observed in the normal mice group with minute notable changes. Variation in morphological effect was more pronounced in organs of the EAC administered group. The kidney of the normal group had the natural architecture of glomerulus with a tuft of capillaries lined by epithelial cells encircled by Bowman's capsule (arrow). The proximal and distal convoluted tubules are lined by simple cuboidal epithelial cells without any hemorrhage (asterisk). The experimental group administered with EAC showed glomerulus degeneration with vacuoles and a shrunken tuft of capillaries lined by epithelial cells with red blood cells, filled with fluid and clear separation of Bowman's capsule (arrow). The proximal and distal convoluted tubules showed tubular degeneration, loss of cytoplasm with proteinaceous fluid in the lumen of the tubules (asterisk). Hyaline casts, renal lesions, and tissue hemorrhages were also noticeable. Animals demonstrated with 5-FU were noticed with mild glomerulus degeneration, the shrunken tuft of capillaries lined by epithelial cells with red blood cells, enclosed by Bowman's capsule (arrow). The proximal and distal convoluted tubules were lined by simple cuboidal epithelial cells with proteinaceous fluid in the lumen (asterisk). These observations of the standard group were also seen in CuO-CP NPs medicated group along with mild hemorrhages between renal tubules.

Histological analysis of sections of liver tissue of normal group revealed the regular architecture of hepatocytes arranged in cord-like fashion surrounding the central vein, hepatocytes with cytoplasm and vesicular nucleus (arrow). There was no sign of cellular regeneration, tubular necrosis, casts, or glomerular congestion. The EAC bearing mice had distortion of the normal appearance of hepatocytes with severe vacuolar degeneration, loss of cytoplasm, condensed with variation size of the vesicular nucleus (arrow), perivascular infiltration of neutrophils, mononuclear cells, and tumor cells (asterisk). Coagulative necrosis, focal angiectasis, and steatosis were also observed in them. The standard group showed the same arrangement as in the normal group but there was mild vacuolar degeneration of hepatocytes (arrow) with perivascular infiltration of neutrophils and mononuclear cells (asterisk) with mild congestion of blood vessels. The CuO-CP NPs dosed group had hepatocytes arranged in cords with moderate perivascular infiltration of neutrophils, and mononuclear cells (asterisk).

The splenic architecture in the normal group had white pulp with lymphocytes (arrow) and red pulp with red blood cells arranged on the reticulum fibers (asterisk). EAC control group had lymphocytes (arrow) and red blood cells (asterisk), but with disarrangement and mild congestions. As for the 5-FU and CuO-CP NP-treated groups, no morphological changes were observed. It was captivating to note that administrating CuO-CP NPs and 5-FU could lower the levels of histopathological changes in laboratory mice affected with ascites tumor. The results of pathological examination evidenced were coincident with the study conducted by (Dhanya et al. 2013; Olayode et al. 2019; Eissa et al. 2019).

Conclusion

From the above investigation, it is evident that extracts of *S. glauca* and *C. paniculatus* being effectively utilized for the synthesis of CuO NPs in a sustainable manner. The phytofabricated CuO NPs confirm their potent anticancer capability against MCF-7 and HT-29 cell lines in a

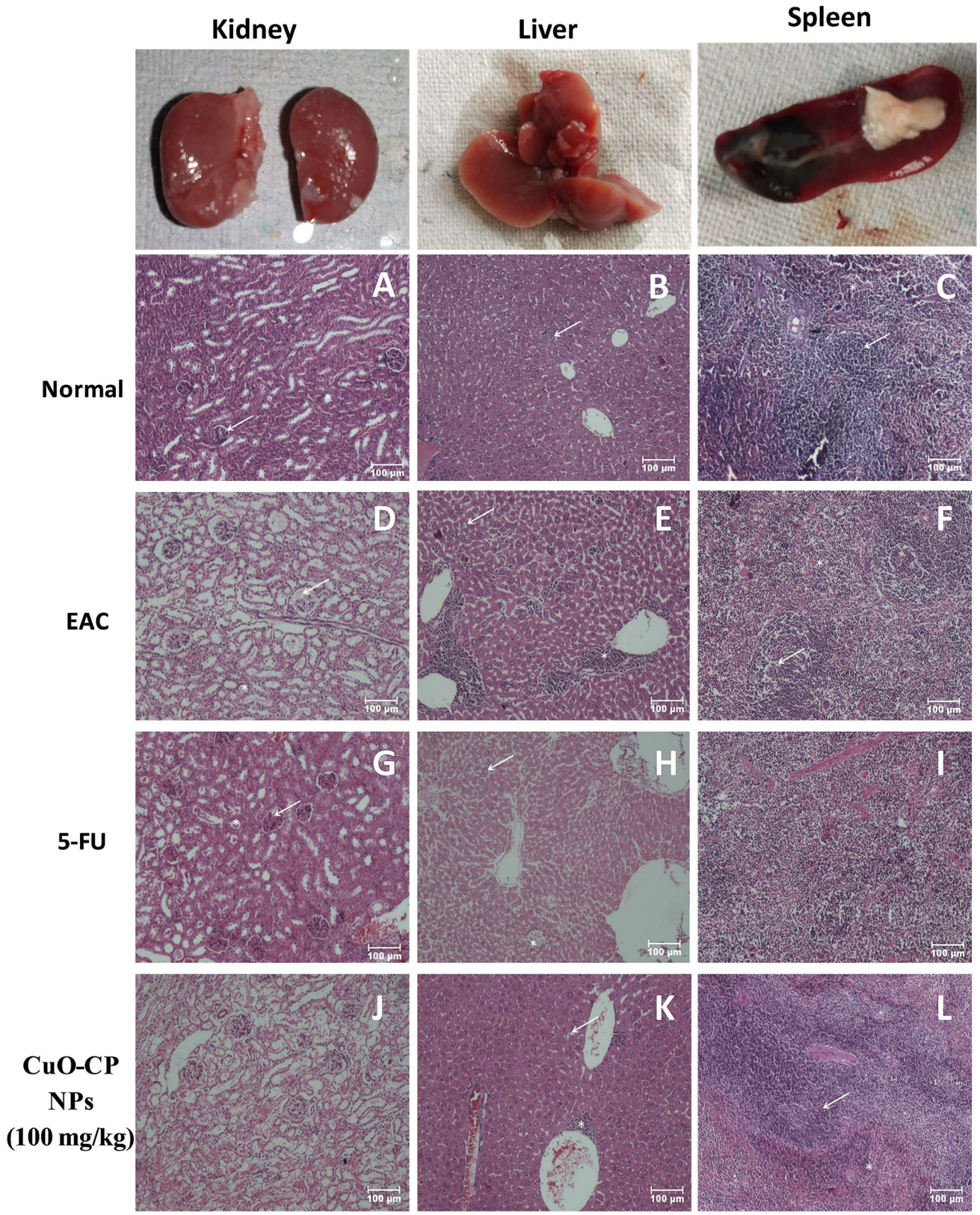

Fig. 10 Images depicting apparent and hematoxylin and eosin staining of kidney (Lane 1: **A**, **D**, **G**, **J**), liver (Lane 2: **B**, **E**, **H**, **K**) and spleen (Lane 3: **C**, **F**, **I**, **L**). signifying retractable changes of CuO-CP NP-treated (**J**, **K**, **L**) compared to standard (**G**, **H**, **I**), EAC induced (**D**, **E**, **F**) and normal laboratory mice (**A**, **B**, **C**)

concentration-dependent manner and CuO-CP NPs treated on MCF-7 cell lines exhibited cell death in the late apoptotic phase. Also, a considerable amount of cells got arrested in the Sub G_0/G_1 phase of the cell cycle when compared with untreated cell control where cells got arrested in a viable (G_0/G_1) phase. The Caspase-3 expression describes that the compound may incorporate the therapeutic potential against human breast cancer. Additionally, the anticancer activity was circumstantiated with in vivo animal studies wherein, the subacute exposure of CuO-CP NPs with 100 mg/kg BW dose could enhance the life span, hematological parameters, biochemical capabilities, and histopathological conditions of EAC induced mice. Thus, the phytofabricated NPs are are very well avowed for favorable anticancer medication.

Supplementary Information The online version contains supplementary material available at https://doi.org/10.1007/s13204-021-01753-3.

Acknowledgments The authors are thankful to Vision Group on Science and Technology, Department of IT, BT and S&T, Government of Karnataka for financial assistance to the Department of Nanotechnology under the K-FIST scheme. Authors are also grateful to UGC for the BSR faculty fellowship to KSR (grant no.F.18-1/2011 (BSR)), Institute of Excellence (IOE) for spectral support at the University of Mysore, Manasagangotri, Mysuru-570006, India. Authors acknowledge the support extended by the expert Plant Taxonomist, Dr. K. Ravikumar, Professor, TDU & Asst. Director for FRLH Herbarium and Raw Drug Repository, FRLHT, Bengaluru for guidance in identifying the plant materials and providing the herbarium certificate for the same and Dr. Takashi Morii, Dr. Arivazhagan Rajendran, and Dr. Shun Nakano, Institute of Advanced Energy, Kyoto University, Uji, Japan, for providing facility to perform TEM analysis.

Compliance with ethical standards

Conflict of interest The authors declare that they have no known conflict or competing financial interests that could have appeared to influence the work which is reported.

References

Abramov OV, Gedanken A, Koltypin Y et al (2009) Pilot scale sonochemical coating of nanoparticles onto textiles to produce biocidal fabrics. Surf Coatings Technol 204:718–722. https://doi.org/10.1016/j.surfcoat.2009.09.030

Ahmed M, Rana A, Dixit V (2005) Calotropis species (*Ascelpediaceace*)—a comprehensive review. Pharmacogn Mag 1:48–52

Alves IABS, Miranda HM, Soares LAL, Randau KP (2014) Simaroubaceae family: botany, chemical composition and biological activities. Rev Bras Farmacogn 24:481–501. https://doi.org/10.1016/j.bjp.2014.07.021

Arya A, Gupta K, Chundawat TS, Vaya D (2018) Biogenic synthesis of copper and silver nanoparticles using green alga *Botryococcus braunii* and its antimicrobial activity. Bioinorg Chem Appl 2018:1–9. https://doi.org/10.1155/2018/7879403

Azizian-Shermeh O, Einali A, Ghasemi A (2017) Rapid biologically one-step synthesis of stable bioactive silver nanoparticles using *Osage orange* (*Maclura pomifera*) leaf extract and their antimicrobial activities. Adv Powder Technol 28:3164–3171. https://doi.org/10.1016/j.apt.2017.10.001

Baghizadeh A, Ranjbar S, Gupta VK et al (2015) Green synthesis of silver nanoparticles using seed extract of *Calendula officinalis* in liquid phase. J Mol Liq 207:159–163. https://doi.org/10.1016/j.molliq.2015.03.029

Bai L, Meng Y, Khan ZA, Zhang V (2017) The synergetic effects of surface texturing and MoDDP additive applied to ball-on-disk friction subject to both flooded and starved lubrication conditions. Tribol Lett 65:163. https://doi.org/10.1007/s11249-017-0949-y

Baik N, seok, Sakai G, Miura N, Yamazoe N, (2000) Preparation of stabilized nanosized tin oxide particles by hydrothermal treatment. J Am Ceram Soc 83:2983–2987. https://doi.org/10.1111/j.1151-2916.2000.tb01670.x

Barbosa LF, Braz-Filho R, Vieira IJC (2011) Chemical constituents of plants from the genus Simaba (Simaroubaceae). Chem Biodivers 8:2163–2178. https://doi.org/10.1002/cbdv.201000323

Berra D, Laouini SE, Benhaoua B et al (2018) Green synthesis of copper oxide nanoparticles by *Pheonix dactylifera* L leaves extract. Dig J Nanomater Biostructures 13:1231–1238

Cheon J, Lee J, Kim J (2012) Inkjet printing using copper nanoparticles synthesized by electrolysis. Thin Solid Films 520:2639–2643. https://doi.org/10.1016/j.tsf.2011.11.021

Das D, Nath BC, Phukon P, Dolui SK (2013) Synthesis and evaluation of antioxidant and antibacterial behavior of CuO nanoparticles. Colloids Surf B Biointerfaces 101:430–433. https://doi.org/10.1016/j.colsurfb.2012.07.002

Dhanya S, Isloor AM, Shetty P, Nayak PG, Pai KSR (2013) In vivo anticancer and histopathology studies of Schiff bases on Ehrlich ascitic carcinoma cells: 1st cancer update. Arab J Chem 6:25–33. https://doi.org/10.1016/j.arabjc.2010.12.016

Dugo EB, Yedjou CG, Stevens JJ, Tchounwou PB (2017) Therapeutic potential of arsenic trioxide (ATO) in treatment of hepatocellular carcinoma: role of oxidative stress in ATO-induced apoptosis. Ann Clin Pathol 5:1101–1128

Eissa MI, El-Sherbiny MA, Ibrahim AM et al (2019) Biochemical and Histopathological studies on female and male Wistar rats fed on genetically modified soybean meals (Roundup Ready). J Basic Appl Zool 80:54. https://doi.org/10.1186/s41936-019-0114-2

El-Far M, Salah N, Essam A et al (2019) Potential anticancer activity and mechanism of action of nanoformulated curcumin in experimental Ehrlich ascites carcinoma-bearing animals. Nanomedicine 14:553–573. https://doi.org/10.2217/nnm-2018-0298

Ellman GL (1959) Tissue sulfhydryl groups. Arch Biochem Biophys 82:70–77. https://doi.org/10.1016/0003-9861(59)90090-6

Elsayed WM, Abdel-Gawad E-HAHA, Mesallam DIAA, El-Serafy TS (2020) The relationship between oxidative stress and acute ischemic stroke severity and functional outcome. Egypt J Neurol Psychiatry Neurosurg 56:1–6. https://doi.org/10.1186/s41983-020-00206-y

Ethiraj AS, Kang DJ (2012) Synthesis and characterization of CuO nanowires by a simple wet chemical method. Nanoscale Res Lett 7:70. https://doi.org/10.1186/1556-276X-7-70

Gopinath V, Priyadarshini S, Al-Maleki AR et al (2016) In vitro toxicity, apoptosis and antimicrobial effects of phyto-mediated copper oxide nanoparticles. RSC Adv 6:110986–110995. https://doi.org/10.1039/C6RA13871C

Harish B, Krishna V, Kumar H et al (2008a) Wound healing activity and docking of glycogen-synthase-kinase-3-β-protein with isolated triterpenoid lupeol in rats. Phytomedicine 15:763–767. https://doi.org/10.1016/j.phymed.2007.11.017

Hassanien R, Husein DZ, Al-Hakkani MF (2018) Biosynthesis of copper nanoparticles using aqueous Tilia extract: antimicrobial and anticancer activities. Heliyon 4:e01077. https://doi.org/10.1016/j.heliyon.2018.e01077

Hwa KY, Karuppaiah P, Gowthaman NSK et al (2019) Ultrasonic synthesis of CuO nanoflakes: a robust electrochemical scaffold for the sensitive detection of phenolic hazard in water and pharmaceutical samples. Ultrason Sonochem 58:104649

Karmakar I, Dolai N, Suresh Kumar RB et al (2013) Antitumor activity and antioxidant property of Curcuma caesia against Ehrlich's ascites carcinoma bearing mice. Pharm Biol 51:753–759. https://doi.org/10.3109/13880209.2013.764538

Kiessling F, Liu Z, Gätjens J et al (2010) Advanced nanomaterials in multimodal imaging: design, functionalization, and biomedical applications. J Nanomater 2010:1–15. https://doi.org/10.1155/2010/894303

Koca FD, Demirezen Yilmaz D, Duman F, Ocsoy I (2018) Comparison of phytotoxic effects of bio-synthesised copper oxide nanoparticle and ionic copper on *Elodea canadensis*. Chem Ecol 34:839–853. https://doi.org/10.1080/02757540.2018.1494162

Kumar KH, Venuprasad MP, Jayashree GV et al (2015) Celastrus paniculatus Willd. mitigates t-BHP induced oxidative and apoptotic damage in C2C12 murine muscle cells. Cytotechnology 67:955–967. https://doi.org/10.1007/s10616-014-9733-0

Kumar KHK, Razack S, IN-IC, et al (2014) Phytochemical analysis and biological properties of *Cyperus rotundus* L. Ind Crops Prod 52:815–826. https://doi.org/10.1039/C8RA07985D

Kumar RS, Almansour AI, Arumugam N et al (2018) Highly functionalized pyrrolidine analogues: stereoselective synthesis and caspase-dependent apoptotic activity. RSC Adv 8:41226–41236

Li Y-MM, Sun S-QQ, Zhou Q et al (2004) Identification of American ginseng from different regions using FT-IR and two-dimensional correlation IR spectroscopy. Vib Spectrosc 36:227–232. https://doi.org/10.1016/j.vibspec.2003.12.009

Li Y, Liang J, Tao Z, Chen J (2008) CuO particles and plates: synthesis and gas-sensor application. Mater Res Bull 43:2380–2385. https://doi.org/10.1016/j.materresbull.2007.07.045

Mathuram TL, Ravikumar V, Reece LM et al (2016) Tideglusib induces apoptosis in human neuroblastoma IMR32 cells, provoking sub-G0/G1 accumulation and ROS generation. Environ Toxicol Pharmacol 46:194–205. https://doi.org/10.1016/j.etap.2016.07.013

Meghana S, Kabra P, Chakraborty S, Padmavathy N (2015) Understanding the pathway of antibacterial activity of copper oxide nanoparticles. RSC Adv 5:12293–12299. https://doi.org/10.1039/C4RA12163E

Mosmann T (1983) Rapid colorimetric assay for cellular growth and survival: application to proliferation and cytotoxicity assays. J Immunol Methods 65:55–63. https://doi.org/10.1016/0022-1759(83)90303-4

Mullane KM, Kraemer R, Smith B (1985) Myeloperoxidase activity as a quantitative assessment of neutrophil infiltration into ischemie myocardium. J Pharmacol Methods 14:157–167. https://doi.org/10.1016/0160-5402(85)90029-4

Munawer U, Raghavendra VB, Ningaraju S et al (2020) Biofabrication of gold nanoparticles mediated by the endophytic *Cladosporium* species: photodegradation, in vitro anticancer activity and in vivo antitumor studies. Int J Pharm 588:29–41. https://doi.org/10.1016/j.ijpharm.2020.119729

Nagajyothi PC, Muthuraman P, Sreekanth TVM et al (2017) Green synthesis: in-vitro anticancer activity of copper oxide nanoparticles against human cervical carcinoma cells. Arab J Chem 10:215–225. https://doi.org/10.1016/j.arabjc.2016.01.011

Nagaonkar D, Shende S, Rai M (2015) Biosynthesis of copper nanoparticles and its effect on actively dividing cells of mitosis in *Allium cepa*. Biotechnol Prog 31:557–565. https://doi.org/10.1002/btpr.2040

Naika HR, Lingaraju K, Manjunath K et al (2015) Green synthesis of CuO nanoparticles using *Gloriosa superba* L. extract and their antibacterial activity. J Taibah Univ Sci 9:7–12. https://doi.org/10.1016/j.jtusci.2014.04.006

Namvar F, Sulaiman Rahman H, Mohammad R, Baharara J, Mahdavi M, Amini E, Stanley Chartrand M, Yeap SK, Namvar F, Rahman HS et al (2014) Cytotoxic effect of magnetic iron oxide nanoparticles synthesized via seaweed aqueous extract. Int J Nanomedicine 9:2479–2488. https://doi.org/10.2147/IJN.S59661

Nasrollahzadeh M, Sajadi SM, Maham M (2015) Tamarix gallica leaf extract mediated novel route for green synthesis of CuO nanoparticles and their application for N-arylation of nitrogen-containing heterocycles under ligand-free conditions. RSC Adv 5:40628–40635. https://doi.org/10.1039/c5ra04012d

Nethravathi PC, Kumar MAP, Suresh D et al (2015) Tinospora cordifolia mediated facile green synthesis of cupric oxide nanoparticles and their photocatalytic, antioxidant and antibacterial properties. Mater Sci Semicond Process 33:81–88. https://doi.org/10.1016/j.mssp.2015.01.034

Ohkawa H, Ohishi N, Yagi K (1979) Assay for lipid peroxides in animal tissues by thiobarbituric acid reaction. Anal Biochem 95:351–358. https://doi.org/10.1016/0003-2697(79)90738-3

Olayode OA, Daniyan MO, Olayiwola G (2019) Biochemical, hematological and histopathological evaluation of the toxicity potential of the leaf extract of *Stachytarpheta cayennensis* in rats. J Tradit Complement Med 10:544–554. https://doi.org/10.1016/j.jtcme.2019.05.001

Patil R, Prakash K, Clinical VM-I, journal of, (2010) U (2010) Hypolipidemic effect of *Celastrus paniculatus* in experimentally induced hypercholesterolemic wistar rats. Springer 25:405–410. https://doi.org/10.1007/s12291-010-0050-x

Rajashekaraiah R, Kumar PR, Prakash N et al (2020) Anticancer efficacy of 6-thioguanine loaded chitosan nanoparticles with or without curcumin. Int J Biol Macromol 148:704–714. https://doi.org/10.1016/j.ijbiomac.2020.01.117

Rajkumar R, Kumar EP, Sudha S, Suresh B (2007) Evaluation of anxiolytic potential of *Celastrus oil* in rat models of behaviour. Fitoterapia 78:120–124. https://doi.org/10.1016/j.fitote.2006.09.028

Ramamurthy N, Kannan S (2007) Fourier transform infrared spectroscopic analysis of a plant (*Calotropis gigantea* Linn) from an industrial village, Cuddalore dt, Tamilnadu, India. Rom J Biophys 17:269–276

Ramaswamy SVP, Narendhran S, Sivaraj R (2016) Potentiating effect of ecofriendly synthesis of copper oxide nanoparticles using brown alga: antimicrobial and anticancer activities. Bull Mater Sci 39:361–364. https://doi.org/10.1007/s12034-016-1173-3

Rao CNR (1963) Chemical applications of infrared spectroscopy. Science. Academic Press, p 1441

Ray asit, Jena S, Dash B, et al (2019) Hedychium coronarium extract arrests cell cycle progression, induces apoptosis, and impairs migration and invasion in HeLa cervical cancer cells. Cancer Manag Res 11:483. https://doi.org/10.2147/CMAR.S190004

Rehana D, Mahendiran D, Kumar RS, Rahiman AK (2017) Evaluation of antioxidant and anticancer activity of copper oxide nanoparticles synthesized using medicinally important plant extracts. Biomed Pharmacother 89:1067–1077. https://doi.org/10.1016/j.biopha.2017.02.101

Saif S, Tahir A, Asim T, et al (2016) Plant mediated green synthesis of CuO nanoparticles: comparison of toxicity of engineered and plant mediated CuO nanoparticles towards Daphnia magna. mdpi.com 6:205. doi: https://doi.org/10.3390/nano6110205

Sari LM, Subita GP, Auerkari EI (2018) Areca nut extract demonstrated apoptosis-inducing mechanism by increased caspase-3 activities on oral squamous cell carcinoma. F1000Research 7:1–34. https://doi.org/10.12688/f1000research.14856.5

Seigneuric R, Markey L, S.A. Nuyten D, et al (2010) From nanotechnology to nanomedicine: applications to cancer research. Curr Mol Med 10:640–652. https://doi.org/10.2174/156652410792630634

Sivaraj R, Rahman PKSMSM, Rajiv P et al (2014a) Biosynthesis and characterization of *Acalypha indica* mediated copper oxide nanoparticles and evaluation of its antimicrobial and anticancer activity. Spectrochim Acta Part A Mol Biomol Spectrosc 129:255–258. https://doi.org/10.1016/j.saa.2014.03.027

Sivaraj R, Rahman PKSMSM, Rajiv P et al (2014b) Biogenic copper oxide nanoparticles synthesis using *Tabernaemontana divaricate* leaf extract and its antibacterial activity against urinary tract pathogen. Spectrochim Acta Part A Mol Biomol Spectrosc 133:178–181. https://doi.org/10.1016/j.saa.2014.05.048

Suárez-Cerda J, Espinoza-Gómez H, Alonso-Núñez G et al (2017) A green synthesis of copper nanoparticles using native cyclodextrins as stabilizing agents. J Saudi Chem Soc 21:341–348. https://doi.org/10.1016/j.jscs.2016.10.005

Sulaiman GM, Tawfeeq AT, Jaaffer MD (2018) Biogenic synthesis of copper oxide nanoparticles using olea europaea leaf extract and evaluation of their toxicity activities: an in vivo and in vitro study. Biotechnol Prog 34:218–230. https://doi.org/10.1002/btpr.2568

Suresh D, Nethravathi PC, Udayabhanu, et al (2015a) Green synthesis of multifunctional zinc oxide (ZnO) nanoparticles using *Cassia fistula* plant extract and their photodegradative, antioxidant and antibacterial activities. Mater Sci Semicond Process 31:446–454. https://doi.org/10.1016/j.mssp.2014.12.023

Suresh D, Udayabhanu NPC et al (2015b) EGCG assisted green synthesis of ZnO nanopowders: photodegradative, antimicrobial and antioxidant activities. Spectrochim Acta Part A Mol Biomol Spectrosc 136:1467–1474. https://doi.org/10.1016/j.saa.2014.10.038

Suresh Y, Annapurna S, Bhikshamaiah G, Singh AK (2016) Green luminescent copper nanoparticles. Mater Sci Eng C 149:12187. https://doi.org/10.1088/1757-899X/149/1/012187

Tarasov S, Kolubaev A, Belyaev S et al (2002) Study of friction reduction by nanocopper additives to motor oil. Wear 252:63–69. https://doi.org/10.1016/S0043-1648(01)00860-2

Thenmozhi T (2020) Functionalization of iron oxide nanoparticles with clove extract to induce apoptosis in MCF-7 breast cancer cells. 3 Biotech 10:82. https://doi.org/10.1007/s13205-020-2088-7

Thylur RP, Senthivinayagam S, Campbell EM et al (2011) Mixed lineage kinase 3 modulates β-catenin signaling in cancer cells. J Biol Chem 286:37470–37482. https://doi.org/10.1074/jbc.m111.298943

Uddandrao VVS, Parim B, Nivedha PR et al (2019) Anticancer activity of pomegranate extract: effect on hematological and antioxidant profile against ehrlich-ascites-carcinoma in Swiss albino mice. Orient Pharm Exp Med 19:243–250

Verma N, Kumar N (2019) Synthesis and biomedical applications of copper oxide nanoparticles: an expanding horizon. ACS Biomater Sci Eng 5:1170–1188. https://doi.org/10.1021/acsbiomaterials.8b01092

Vishveshvar K, Aravind Krishnan MV, Haribabu K et al (2018) Green synthesis of copper oxide nanoparticles using Ixiro coccinea plant leaves and its characterization. Bionanoscience 8:554–558. https://doi.org/10.1007/s12668-018-0508-5

Wadhwa R, Aggarwal T, Thapliyal N et al (2019) Red blood cells as an efficient in vitro model for evaluating the efficacy of metallic nanoparticles. 3 Biotech 9:279. https://doi.org/10.1007/s13205-019-1807-4

Wang X, Wang L, Fu Y et al (2013) Promising effects on ameliorating mitochondrial function and enhancing Akt signaling in SH-SY5Y cells by (M)-bicelaphanol A, a novel dimeric podocarpane type. Phytomedicine 20:1064–1070. https://doi.org/10.1016/j.phymed.2013.04.017

Weng JJ-R, Yen M-HM, Lin W-Y et al (2013) Cytotoxic constituents from *Celastrus paniculatus* induce apoptosis and autophagy in breast cancer cells. Phytochemistry 94:211–219. https://doi.org/10.1016/j.phytochem.2013.05.022

WHO 2018 (2018) Latest global cancer data: Cancer burden rises to 18.1 million new cases and 9.6 million cancer deaths in 2018

Xie W, Zhang Z, Liao L et al (2020) Green chemical mechanical polishing of sapphire wafers using a novel slurry. Nanoscale 12:22518–22526. https://doi.org/10.1039/D0NR04705H

Ye T, Guiwen Z, Weiping Z, Shangda X (1997) Combustion synthesis and photoluminescence of nanocrystalline Y2O3: Eu phosphors. Mater Res Bull 32:501–506. https://doi.org/10.1016/S0025-5408(97)00007-X

Zhang Z, Cui J, Wang B et al (2017) A novel approach of mechanical chemical grinding. J Alloys Compd 726:514–524. https://doi.org/10.1016/j.jallcom.2017.08.024

Zhang Z, Cui J, Zhang J et al (2019) Environment friendly chemical mechanical polishing of copper. Appl Surf Sci 467–468:5–11. https://doi.org/10.1016/j.apsusc.2018.10.133

Zhang Z, Guo D, Wang B et al (2015) A novel approach of high speed scratching on silicon wafers at nanoscale depths of cut. Sci Rep 5:16395. https://doi.org/10.1038/srep16395

Zhang Z, Huo F, Zhang X, Guo D (2012) Fabrication and size prediction of crystalline nanoparticles of silicon induced by nanogrinding with ultrafine diamond grits. Scr Mater 67:657–660. https://doi.org/10.1016/j.scriptamat.2012.07.016

Zhang Z, Huo Y, Guo D (2013) A model for nanogrinding based on direct evidence of ground chips of silicon wafers. Sci China Technol Sci 56:2099–2108. https://doi.org/10.1007/s11431-013-5286-2

Zhang Z, Liao L, Wang X et al (2020) Development of a novel chemical mechanical polishing slurry and its polishing mechanisms on a nickel alloy. Appl Surf Sci 506:144670. https://doi.org/10.1016/j.apsusc.2019.144670

Zhang Z, Liu J, Hu W et al (2021) Chemical mechanical polishing for sapphire wafers using a developed slurry. J Manuf Process 62:762–771. https://doi.org/10.1016/j.jmapro.2021.01.004